First-principles theory of ionic diffusion with nondilute carriers

A. Van der Ven and G. Ceder
Department of Materials Science and Engineering, Massachusetts Institute of Technology, Cambridge, Massachusetts 02139

M. Asta
Department of Materials Science and Engineering, Northwestern University, Evanston, Illinois 60208

P. D. Tepesch
Corning, Inc., Corning, New York 14831

(Received 6 April 2001; revised manuscript received 12 July 2001; published 25 October 2001)

Many multicomponent materials exhibit significant configurational disorder. Diffusing ions in such materials migrate along a network of sites that have different energies and that are separated by configuration dependent activation barriers. We describe a formalism that enables a first-principles calculation of the diffusion coefficient in solids exhibiting configurational disorder. The formalism involves the implementation of a local cluster expansion to describe the configuration dependence of activation barriers. The local cluster expansion serves as a link between accurate first-principles calculations of the activation barriers and kinetic Monte Carlo simulations. By introducing a kinetically resolved activation barrier, we show that a cluster expansion for the thermodynamics of ionic disorder can be combined with a local cluster expansion to obtain the activation barrier for migration in any configuration. This ensures that in kinetic Monte Carlo simulations, detailed balance is maintained at all times and kinetic quantities can be calculated in a properly equilibrated thermodynamic state. As an example, we apply this formalism for an investigation of lithium diffusion in Li_xCoO_2. A study of the activation barriers in Li_xCoO_x within the local density approximation shows that the migration mechanism and activation barriers depend strongly on the local lithium-vacancy arrangement around the migrating lithium ion. By parametrizing the activation barriers with a local cluster expansion and applying it in kinetic Monte Carlo simulations, we predict that lithium diffusion in layered Li_xCoO_2 is mediated by divacancies at all lithium concentrations. Furthermore, due to a strong concentration dependence of the activation barrier, the predicted diffusion coefficient varies by several orders of magnitude with lithium concentration x.

DOI: 10.1103/PhysRevB.64.184307 PACS number(s): 61.50.Ah, 64.60.Cn, 81.30.Dz, 84.60.Dn

I. INTRODUCTION

Diffusion of atoms and ions is an important kinetic property of many materials. It determines whether stable states can be reached and at which rate this can occur. Many technologically relevant materials rely on low diffusion rates to prevent them from evolving to their equilibrium, but often less useful, state. For example, corrosion of some materials is limited by oxygen or cation transport through a surface phase. In other technologically important materials, fast ionic diffusion is desirable. This is the case in materials for ionic membranes,[1] solid electrolytes,[2,3] and insertion electrodes.[4,5]

Ionic diffusion in crystalline solids typically occurs by diffusion-mediating defects such as vacancies or interstitials. Often these carriers of diffusion are present at a very low concentration such that they do not interact. In this regime, dilute diffusion theory is valid and the diffusivity can be written as

$$D = a^2 g f x_D \nu^* \exp\left(\frac{-\Delta E_a}{kT}\right), \tag{1}$$

where a is a hop distance, g is a geometric factor, f is a correlation factor, and x_D is the concentration of the diffusion-mediating defect. ΔE_a is the activation barrier which is defined as the difference in energy at the activated state and the energy at the initial state of the ionic hop. The factor ν^* has the dimension of a frequency and is determined by the difference in entropy at the activated state and the initial equilibrium state of the hop.

For many important materials dilute-diffusion theory breaks down. This occurs when the concentration of carriers (i.e., vacancies or interstitials) is sufficiently large that they interact. Such interactions can lead to short range or even long-range order among the diffusion-mediating defects, complicating an analysis of diffusion. Along its trajectory, the migrating ion will sample different local environments and each hop will be characterized by a different activation barrier ΔE_a. Furthermore, at each step of the migration the diffusing species may have a different concentration of mediating defects in its vicinity.

Nondilute diffusion is common in technologically important materials. Examples include doped zirconias for fuel cells[1] or perovskites for oxygen membranes (e.g., $SrCoO_{3-\delta}$). In these compounds, large oxygen-vacancy concentrations can be obtained, enhancing the possibility of order-disorder transitions between oxygen ions and vacancies, and thereby significantly affecting the mobility of the diffusing oxygen ions. Lithium insertion oxides,[6] used as electrodes in lithium-ion batteries are another example. In battery charging and discharging, lithium ions are inserted in and removed from interstitial sites in a transition-metal oxide host. During this process, the host undergoes a wide range of lithium concentrations and many different degrees of lithium order and disorder are sampled.

In this paper, we present a formalism to study diffusion in nondilute systems from first principles. The approach makes use of a local cluster expansion to parametrize the environment dependence of the activation barrier. Periodic cluster expansions have proven to be an invaluable tool for the investigation of thermodynamic properties in multicomponent systems exhibiting configurational disorder.[7,8] It is commonly implemented for the calculation of binary phase diagrams of systems in which the different species can be ordered or disordered on a common crystal structure.[9–20] The power of a cluster expansion lies in its ability to accurately and with minimal computational cost extrapolate first-principles energy values of a relatively few, small periodic arrangements of ions in a given crystal structure, to the energy of any ionic configuration within the same crystal structure. In the present context of diffusion in nondilute systems, we show how the cluster expansion formalism can be cast in a form to parametrize arrangement-dependent activation barriers calculated from first principles. The resulting *local cluster expansion* for the activation barrier can then be combined with a cluster expansion for the configurational energy of the solid in kinetic Monte Carlo simulations to investigate diffusion in nondilute systems. Such a kinetic Monte Carlo simulation will contain both accurate kinetic as well as thermodynamic information.

As an illustration, we implement this approach in the study of lithium diffusion in Li_xCoO_2. We find that the local arrangement around migrating lithium ions plays an essential role in determining both the hopping mechanism and the value of the activation barrier. The paper is divided in two parts. The first part (Sec. II) focuses on the formalism and introduces the local cluster expansion to describe the configuration dependence of the activation barrier. In the second part (Sec. III), the formalism is applied to Li_xCoO_2. Preliminary results of our study of lithium diffusion in Li_xCoO_2 have been published previously.[21] Here we elaborate on those results and focus in depth on the computational details to illustrate the formalism described in Sec. II.

II. METHODOLOGY

A. Diffusion coefficient

We consider the diffusion of a single type of species on a subset of sites of the crystal structure of a host and assume that migration occurs by the exchange with adjacent vacant sites. This is a common mechanism for diffusion in many oxides and in some metals with interstitial components: In doped zirconias and defective perovskites such as $SrCoO_{3-\delta}$, oxygen diffusion occurs by exchanges with vacancies on the oxygen sublattice; in fast ion conductors such as sodium-β'' alumina or insertion electrodes such as Li_xCoO_2, the sodium ions and lithium ions respectively migrate along two-dimensional interstitial sublattices within the oxide host by exchanges with adjacent vacancies; and finally, in steel, the carbon atoms reside and diffuse on the interstitial sites of bcc iron. We will denote these systems by A_xB where A is the diffusing species, B is the formula unit of the host and x is the ratio of A to the number of available sites for A within the host B.

A measure of the mobility of a particular species in a host structure is the chemical diffusion coefficient D_c which relates the flux $\mathbf{J}$ of that species to its concentration gradient according to Fick's law

$$\mathbf{J} = -D_c \vec{\nabla} C. \tag{2}$$

C is the concentration x of the diffusing species divided by the volume of A_xB and D_c is the diffusion tensor. On the microscopic level the chemical diffusion coefficient can be determined at equilibrium with[22–24]

$$D_c = \Theta D_J, \tag{3}$$

where

$$\Theta = \left(\frac{\langle (\delta N)^2 \rangle}{\langle N \rangle} \right)^{-1} = \left(\frac{\partial(\mu/kT)}{\partial \ln x} \right) \tag{4}$$

is called the thermodynamic factor and

$$D_J = \lim_{t\to\infty} \left[\frac{1}{2dt} \left\langle \frac{1}{N} \left(\sum_{i=1}^{N} \vec{r}_i(t) \right)^2 \right\rangle \right] \tag{5}$$

is referred to as the jump diffusion coefficient.[22,26] N corresponds to the number of diffusing ions, $\vec{r}_i(t)$ is the displacement of the ith ion after time t, and d is the dimension of the lattice on which diffusion takes place. $\langle \delta N^2 \rangle$ is the fluctuation in the particle number of the diffusing species in an open system. In a closed system, it can be approximated by the fluctuation in a region of average $\langle N \rangle$ particles. μ is the chemical potential of the diffusing species at concentration x. Equations (3), (4), and (5) together form the Kubo-Green equation for diffusion.[22–24]

The jump diffusion coefficient D_J of Eq. (3), which can be considered as a kinetic quantity, is related to the displacement of the *center of mass of all the diffusing ions*. The thermodynamic factor Θ is related to the chemical potential μ according to the second equality in Eq. (4). Θ accounts for the deviation from ideality of the diffusing species in a solid solution with the host in which it is diffusing. The occurrence of a thermodynamic factor in Eq. (3) arises from the fact that the true driving force for diffusion is a gradient in chemical potential[25] and not a gradient in concentration as is assumed in Fick's law (2). The thermodynamic factor, therefore, accounts for the difference between a gradient in concentration and a gradient in chemical potential. Only for ideal solutions and in the dilute concentration limit, where the chemical potential of the diffusing species at concentration x assumes the form $\mu = \mu^0 + kT \ln(x)$, does the thermodynamic factor equal 1.

Another useful quantity to characterize ion mobility is the more common tracer diffusion coefficient which is defined as[22]

$$D^* = \lim_{t\to\infty} \left[\frac{1}{2dt} \left(\frac{1}{N} \sum_{i=1}^{N} \langle [\vec{r}_i(t)]^2 \rangle \right) \right]. \tag{6}$$

D^* differs from D_J in that it measures the square of the displacement of individual particles as opposed to the square

of the displacement of the center of mass of all the diffusing ions. If on average, there are no cross correlations between displacements $\vec{r}_i(t)$ of different particles at different times, D_J and D^* become equivalent.[22,23] Monte Carlo studies of diffusion for simple lattice models on a square lattice indicate that D^* is typically of the same order of magnitude as D_J though not exactly equal to it.[26]

To obtain the displacements $\vec{r}_i(t)$ appearing in Eqs. (5) and (6) for the ions i, a dynamics has to be defined for the system. While in principle, molecular dynamics can be used to generate $\vec{r}_i(t)$, for most systems diffusion is too slow to be efficiently captured on the short time scales of such simulations. For hopping diffusion, a kinetic Monte Carlo model (KMC) can be used where ions hop between preselected sites and by predetermined mechanisms. By randomly selecting ions and letting them hop with correct relative probabilities, a ''dynamical'' trajectory for the $\vec{r}_i(t)$ can be calculated. Implicit in this approach is the assumption that sufficient time elapses between different hops such that the ions are completely thermalized before they execute the next hop. This means that correlations between successive hops are negligible and diffusion can be considered a stochastic process (i.e., Markovian). Such an assumption is valid for most solids[27] with the exception of those exhibiting liquidlike diffusion.

During each hop, the migrating ion crosses an energy barrier, often referred to as a dividing surface, that separates the energy wells constituting the end points of the hop. This dividing surface contains the activated state of the hop which corresponds to a saddle point in the energy of the solid. The activation barrier ΔE_a of a hop is defined as

$$\Delta E_a = E_{\mathrm{AS}} - E_i , \tag{7}$$

where E_i is the energy of the crystal in the initial state and E_{AS} is the energy of the crystal with the hopping ion in the activated state. The frequency Γ with which a hop occurs is well approximated by transition state theory[28] which states that

$$\Gamma = \nu \exp\left(\frac{\Delta S_a}{k}\right)\exp\left(\frac{-\Delta E_a}{kT}\right). \tag{8}$$

ΔS_a is the activation entropy and can be written as[29,30]

$$\Delta S_a = k \ln\left(\frac{(\Delta\psi)^{-1}\int d\psi \exp[-(E-\Delta E_a)/kT]}{(\Delta\zeta)^{-1}\int d\zeta \exp(-E/kT)}\right), \tag{9}$$

where ψ and ζ are generalized coordinates (spatial coordinates of the ions multiplied by the square root of their mass[28,29]) and E is the energy as a function of these generalized coordinates. For a solid with M ions, the integral in the numerator proceeds over a $(3M-1)$-dimensional dividing surface while the integral in the denominator spans a $3M$-dimensional volume around the initial state of the hop. $\Delta\psi$ and $\Delta\zeta$ are integration volumes along the dividing surface and around the initial state of the hop, respectively. ν in Eq. (8) is an effective frequency and is equal to $(kT/2\pi)^{1/2}(\Delta\psi/\Delta\zeta)$.

As with the activation barrier ΔE_a, Eq. (9) suggests that the activation entropy ΔS_a can be written as

$$\Delta S_a = S_{\mathrm{AS}} - S_i , \tag{10}$$

where S_i corresponds to k times the logarithm of the denominator in Eq. (9) and S_{AS} corresponds to k times the logarithm of the numerator in Eq. (9). The dominant contribution to the nonconfigurational entropy change ΔS_a is vibrational entropy. The prefactor of Eq. (8)

$$\nu^* = \nu \exp\left(\frac{\Delta S_a}{k}\right) \tag{11}$$

has the dimension of a frequency and is typically assumed to be of the order of 10^{13} Hz. Nevertheless, examples exist, such as the two dimensional diffusion on a Ge surface, where the prefactor was found from first principles to be between 10^{11} and 10^{12} Hz.[31]

The fundamental assumption of transition state theory is that all trajectories originating in the energy well of the initial state of the hop and crossing the dividing surface continue to the final state of the hop. In reality, though, a subset of trajectories exist that recross the dividing surface and return to the initial state. Transition state theory neglects the flux of recrossing trajectories and, therefore, gives an upper bound to the true hopping rate. To correct this discrepancy, the migration rate of transition state theory is sometimes multiplied by a recrossing coefficient, κ, which typically ranges between 0.1 and 1. The value of the recrossing coefficient depends on the details of the energy surface.[33,34] Several techniques to estimate the recrossing coefficient have been developed for diffusion in solids.[32–36] For simplicity we will set $\kappa = 1$, keeping in mind that the hopping rate of transition state theory, Eq. (8), gives an upper bound to the true hopping rate.

B. Configuration dependence of the energy and activation barrier

In this paper, we are concerned with solids in which the diffusing species resides on a subset of crystallographic sites within a host and in which diffusion is mediated by vacancies. We will refer to this subset of crystallographic sites as Σ. In the nondilute regime, in which the diffusing species shares the sites of Σ with a large concentration of vacancies, there exists a degree of disorder on Σ. Different arrangements of ions on Σ can occur and each arrangement typically has a different energy. At finite temperature, the configuration of ions on Σ evolve over time as a result of the thermally activated hops of ions on Σ to adjacent vacant sites on Σ.

Not only is the energy of the solid dependent on the arrangement of ions and vacancies on Σ, but the energy of the solid when a diffusing ion is at an activated state E_{AS} also depends on the surrounding configuration on Σ. It is well known that the configurational energy of the solid E_i can

rigorously be described with a lattice model formalism.[7,8,37,38] By assigning occupation variables to each site on Σ which are $+1$ (-1) if a diffusing species (vacancy) resides at that site, it is possible to describe the configurational energy of the solid with a cluster expansion[7]

$$E = V_0 + \sum_{\alpha} V_{\alpha} \phi_{\alpha}, \tag{12}$$

where

$$\phi_{\alpha} = \prod_{i \in \alpha} \sigma_i. \tag{13}$$

The polynomials ϕ_{α} are equal to products of occupation variables corresponding to clusters α of sites i of Σ. The clusters α refer to figures of sites on Σ which include for example, nearest neighbor pair clusters, second nearest neighbor pair clusters, triplets of sites, etc. It can be shown that the expansion is exact when it extends over all possible clusters of sites,[7] but to be practical, it must be truncated after a polynomial corresponding to some maximal sized cluster. The coefficients V_0 and V_{α} are referred to as effective cluster interactions (ECI) and are to be determined from first principles. Symmetry is often useful to simplify Eq. (12). Any group of clusters $\alpha, \beta, \ldots$, that are equivalent by the space group symmetry of the crystal have ECI with the same numerical value.[8]

The advantage of a cluster expansion is that it enables a rapid calculation of the configurational energy of the crystal for any arbitrary configuration on Σ. With the above definition of the occupation variables σ_i for each site i, a particular configuration on Σ can be represented by an array of $+1$ and -1's. To calculate the energy then, all that is required is that the polynomials ϕ_{α} for the different clusters α appearing in the cluster expansion be evaluated for this particular configuration. The polynomials can then be multiplied by their corresponding ECI V_{α} and added according to Eq. (12) to obtain the configurational energy of the solid.

The accuracy of the cluster expansion depends on the degree of convergence before it is truncated. There are several ways to determine the ECI, V_{α}, from first principles. Typically, the energies of a set of periodic structures with different ionic configurations are calculated with a first-principles method. A truncated form of Eq. (12) is then inverted with either a least squares procedure[39] or a method based on linear programming[40] to calculate the values of the ECI. The effects of relaxations of the ions on Σ and of the host structure are implicitly accounted for if the energies used in the fit correspond to those of fully relaxed structures. Other approaches for the determination of ECI have also been proposed.[41]

For activation barriers, a description of their configuration dependence with a lattice model formalism is less straightforward than that of the configurational energy. An activation barrier depends not only on the surrounding configuration, but also on the direction in which the ion migrates between the end points of the hop. This is illustrated in Fig. 1. The hop in Fig. 1 is characterized by two end points, but in general, hops can be characterized by $n>2$ end points whereby the hopping ion once at the activated state can choose to continue to any one of the n end points.

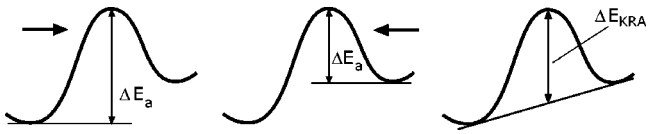

FIG. 1. The activation barrier ΔE_a depends on the direction of the hop (indicated by the arrow). The kinetically resolved activation barrier, ΔE_{KRA}, however, is independent of the direction of the hop.

To overcome the difficulties associated with the direction dependence of ΔE_a, we introduce a kinetically resolved activation (KRA) barrier ΔE_{KRA} whereby the average of the energies of the end points of the hop are subtracted from the energy at the activated state E_{AS} according to

$$\Delta E_{\mathrm{KRA}} = E_{\mathrm{AS}} - \frac{1}{n} \sum_{j=1}^{n} E_{e_j}. \tag{14}$$

E_{e_j} is the energy of the crystal when the migrating ion is at end point j of the hop and the remaining $n-1$ end points of the hop are vacant. Figure 1 schematically illustrates the meaning of ΔE_{KRA} for a hop with two end points. For each of the terms appearing in Eq. (14), the configuration on Σ, excluding the end points of the hop are the same. Subtracting the term $(1/n)\Sigma_{j=1}^{n} E_{e_j}$ from E_{AS} is a way of separating an effective configurational energy, where ions reside only on sites of Σ, from a kinetic component determined when an ion resides at the activated state and the end points of the hop are all vacant. The resulting kinetically resolved activation barrier ΔE_{KRA}, which is still configuration dependent, is independent of the direction of the hop.

Once ΔE_{KRA} and the configurational energy of the solid E_{e_j} for $j=1,n$ are known, it is straightforward to reconstruct the activation barrier for a hop that starts from one of the end points, say $j=1$ according to

$$\Delta E_a = \Delta E_{\mathrm{KRA}} + \frac{1}{n}\left(\sum_{j=1}^{n} E_{e_j} \right) - E_{e_1}. \tag{15}$$

Note that ΔE_{KRA} is equal to ΔE_a when the energies of the n end points are all the same. When the energies of the end points are not equal, ΔE_{KRA} reduces to the average of all the ΔE_a seen from each of the n end points of the hop.

This construction yields a quantity ΔE_{KRA} that depends on the configuration around the migrating ion, but that is independent of the direction of the hop. ΔE_{KRA} can, therefore, be described with a cluster expansion

$$\Delta E_{\mathrm{KRA}} = K_0 + \sum_{\alpha} K_{\alpha} \phi_{\alpha}, \tag{16}$$

As in Eq. (12) ϕ_{α} are polynomials of occupation variables, and K_{α} are kinetic effective cluster interactions (KECI) describing the variation of the kinetically resolved activation barrier with configuration. When a migrating ion is at the activated state, the n end points of the hop are unoccupied.

Assuming that Σ has L sites, the cluster expansion, Eq. (16), then extends over the $L-n$ sites that do not overlap with the n end points of the hop.

The cluster expansion of Eq. (16) enables a rapid calculation of ΔE_{KRA} for any arrangement of ions surrounding the end points of a particular hop. Once a configuration on Σ is specified by assigning values to the occupation variables σ_i, the polynomials ϕ_α can be evaluated for all clusters α appearing in Eq. (16). Multiplying the evaluated polynomials with their corresponding KECI K_α and adding according to Eq. (16) yields the ΔE_{KRA} for the hop of interest surrounded by the given configuration.

A distinction must be made between a cluster expansion of the configurational energy as represented by Eq. (12) and a cluster expansion for the kinetically resolved activation barrier ΔE_{KRA}. The configurational energy is a global extensive property, characterizing the total energy of the whole solid as a function of the arrangement of diffusing ions and vacancies on Σ. ΔE_{KRA}, in contrast, is a local property. This has implications as to how symmetry is to be used to identify clusters with identical KECI in Eq. (16). Equivalent clusters in the cluster expansion for the energy [Eq. (12)] are determined by applying the symmetry elements of the space group of the crystal. For the local cluster expansion [Eq. (16)], the appropriate symmetry operations belong to the highest point group that maps the cluster of n end points of the hop onto itself, with the additional requirement that the point group is consistent with the space group of the solid. Since activation barriers are a local property, it is reasonable to expect that the KECI K_α of Eq. (16) will converge for clusters α that extend beyond a maximal distance away from the hopping ion. The terms in Eq. (16) that correspond to these large clusters can then be neglected.

Local cluster expansions have been used in different contexts to describe the configuration dependence of the local magnetic moments[42] and local vibrational modes[43] in metallic systems. Recently a local cluster expansion was invoked to study the configuration dependence of vacancy formation energies in oxides.[44]

The exponential prefactor ν^* given by Eq. (11) also depends on the local environment. In a similar way as with the activation barrier, we can introduce a kinetically resolved activation entropy ΔS_{KRA}. The essential ingredients to describe the configuration dependence of the activation entropy ΔS_a are a cluster expansion for the nonconfigurational entropy and a local cluster expansion for ΔS_{KRA}. The true activation entropy for the hop ΔS_a can then be reconstructed for any configuration in the same way as was described above for ΔE_a using Eq. (15). Cluster expansions of vibrational entropy and free energy have been explored by Garbulsky and Ceder[45] and Ozolins *et al.*[46]

C. First-principles total energy calculations

The accuracy of a cluster expansion depends on the first-principles method used to derive the ECI of the expansion. A commonly used first-principles method is density functional theory (DFT) within the local density approximation (LDA).[47,48] Many phase diagram calculations drawing on the cluster expansion formalism have relied on DFT-LDA calculations to obtain numerical values for the ECI.[9–20] These studies have shown that DFT-LDA is capable of producing qualitatively accurate predictions of the configurational thermodynamic properties of binary and pseudobinary systems. Often the quantative accuracy of predicted structural properties such as lattice parameters and thermodynamic properties such as order-disorder transition temperatures are good, considering that no experimental input is used.

In the present study, we have used the Vienna *ab initio* simulation package (VASP) (Refs. 49,50) to calculate total energies of solids. This code solves the DFT-LDA Kohn-Sham equations within the pseudopotential approximation[51] whereby the valence electrons are expanded in a plane wave basis set and the effect of the core states on the valence electrons are treated with ultrasoft pseudopotentials.[52] This method is restricted to calculations in systems that are characterized by a periodic cell. To calculate activation barriers with this method, therefore, it is necessary to work with periodic supercells that are large enough to minimize the interaction between the periodic images of the ion in the activated state.

Several ways exist to calculate energies along the migration path. In this work, we have used two. The first is called the elastic band method which enables the determination of the minimum energy path between two energetically stable end points.[53] It starts with a discretized path of on the order of 8-16 replicas of the system that are intermediate between the initial and final states of the path. The replicas are obtained by linear interpolation. A global energy minimization, using the pseudopotential method, is then performed with respect to ionic positions in each replica whereby the coordinates of each replica are connected to those of its neighboring replicas in the interpolation sequence by a spring. The working of the algorithm can be compared to the tightening of an elastic band accross a saddle point between two minima of the energy landscape.

The elastic band method is useful to identify the migration path and the location of the activated state. Nevertheless, to obtain an accurate approximation of the energy at the activated state, a large number of replicas are needed. In many cases, the activated state is located at a high symmetry point between the end points and a calculation of the activation barrier can be performed with the hopping ion initially placed at the high symmetry point. During minimization of the energy of the supercell, the ion will remain at the high symmetry position and the resulting minimum energy will give the best approximation of the activation barrier within the supercell approach.

D. Kinetic Monte Carlo simulations

The kinetic Monte Carlo method enables the numerical calculation of the diffusion coefficients D_c, D_J, and D^* of Eqs. (3),(5),(6) by explicit stochastic simulations of the migration of a collection of ions within a host.[54–62] This is possible provided that the probabilities for individual hops given by Eq. (8) are available. With first principles cluster expansions to calculate the activation barriers ΔE_a of Eqs.

(7) and (15), such hopping probabilities in any environment can be obtained with minimal computational cost.

The basic algorithm implemented in this work is based on the *n*-fold way Monte Carlo algorithm[63] and can be summarized as follows.[54,62] At fixed ion and vacancy concentration on Σ and fixed temperature, the simulation starts with a typical ion-vacancy arrangement exhibiting the equilibrium state of short-range or long-range order. These initial configurations can be obtained with standard equilibrium Monte Carlo techniques in the canonical or grand canonical ensemble using the cluster expansion for the configurational energy. The kinetic Monte Carlo simulation then consists of the repetition of three steps as outlined by Bulnes *et al.*[62] (i) First, all possible migration probabilities Γ_m are determined where m scans the collection of migration paths available to the different migrating ions on Σ. Γ_m is zero if the end points of migration path m are simultaneously occupied. When this is not the case, Γ_m is calculated with the hop frequency of Eq. (8). (ii) In the second step, a random number ρ of the interval (0,1) is sampled. The migration event k is chosen such that

$$\frac{1}{\Gamma_{\text{tot}}}\sum_{m=1}^{k-1}\Gamma_m<\rho\leqslant\frac{1}{\Gamma_{\text{tot}}}\sum_{m=1}^{k}\Gamma_m, \tag{17}$$

where Γ_{tot} is the sum of all individual probabilities Γ_m. This ensures that each event m occurs with probability $\Gamma_m/\Gamma_{\text{tot}}$. The third step (iii) consists of an update of the time Δt leading up to the hop of step (ii). This time is given by

$$\Delta t=-\frac{1}{\Gamma_{\text{tot}}}\ln\zeta \tag{18}$$

with ζ a random number from (0,1).

A kinetic Monte Carlo step (KMCS) is defined as the repetition of steps (i)–(iii) as many times as there are ions on Σ in the simulation. Typically of the order of 10^3 KMCS are required at each temperature and concentration. To obtain adequate averages for D_J and D^*, a series of different initial equilibrium configurations on Σ are essential at each temperature and concentration. Initial configurations on Σ that are representative of equilibrium can be generated with canonical Monte Carlo simulations. Time averages of the different diffusion coefficients can also be performed as described in Ref. 64.

Bulnes *et al.*[62] demonstrated theoretically as well as with a numerical comparison, that the above described kinetic Monte Carlo algorithm is equivalent with the dynamic Monte Carlo algorithm commonly implemented in diffusion studies of lattice models.[57,59,26] The advantage of the above algorithm is that a hop occurs during every sequence of steps (i)–(iii). This is especially advantageous for systems with strongly varying activation barriers. The calculation of the thermodynamic factor Θ of Eq. (3) can occur with grand canonical Monte Carlo simulations.[65]

III. APPLICATION TO LITHIUM DIFFUSION IN Li_xCoO_2

In the remainder of the paper, we implement the above formalism to study lithium diffusion in Li_xCoO_2. This compound is an important cathode material for rechargeable lithium batteries.[66,67] Li_xCoO_2 has a layered crystal structure as illustrated in Fig. 2. It consists of close packed oxygen planes stacked with an *ABCABC* sequence. Alternating between close packed oxygen planes are layers of lithium ions and cobalt ions which reside in the octahedral interstitial sites of the oxygen framework. Both the lithium and cobalt ions form two-dimensional triangular lattices. The particular cation ordering in $LiCoO_2$ produces a crystal with rhombohedral symmetry that belongs to the $R\bar{3}m$ space group. In an electrochemical cell, the lithium ions can be removed from and reinserted into the lithium planes of $LiCoO_2$, resulting in the creation and annihilation of lithium vacancies. Lithium migration through the layered metal oxide host proceeds by exchanges with adjacent vacancies within the same lithium plane. Although variations of x are typically limited between 0.5 and 1.0 when Li_xCoO_2 is used in a commercial battery,[66,68,69] laboratory experiments have demonstrated that almost all the lithium ions can be removed electrochemically from the CoO_2 host.[70] The ability to vary the lithium concentration x in Li_xCoO_2 over large intervals makes this an ideal material to investigate the concentration dependence of diffusion.

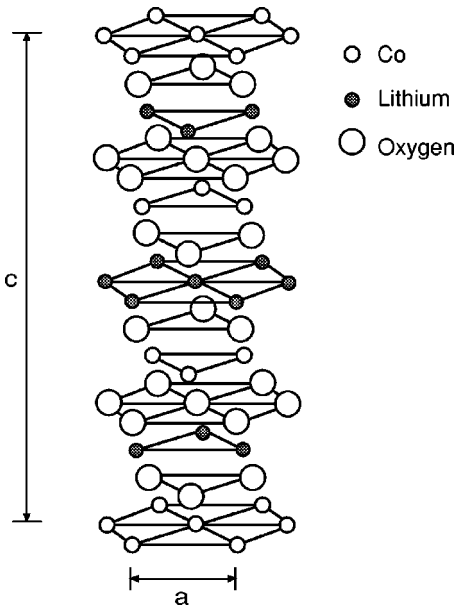

FIG. 2. The $O3$ crystal structure of Li_xCoO_2.

As the lithium concentration varies in Li_xCoO_2, the compound undergoes a series of phase transformations that include order-disorder reactions,[68] a first-order phase transformation[68,69] induced by a metal-insulator transition[19,71] and a series of transformations where the CoO_2 host undergoes structural changes.[70,72] Furthermore, the concentration dependence of thermodynamic properties such as the lithium chemical potential or the equilibrium lattice parameters exhibit strong deviations from ideality.[68–70] These phenomena can be expected to have interesting effects on the evolution of the lithium diffusion coefficient with concentration.

Although different polymorphs of layered Li_xCoO_2 exist, in this paper, we restrict ourselves to a study of diffusion in

the $O3$ form of Li_xCoO_2, the most important polymorph of Li_xCoO_2. This is the polymorph that is described above and is illustrated in Fig. 2. The thermodynamic properties of layered Li_xCoO_2 have previously been investigated from first principles using the cluster expansion formalism.[19]

Our study of lithium diffusion in Li_xCoO_2 entailed three steps. First we identified the different possible lithium migration mechanisms from first principles using the pseudopotential method in the local density approximation (as implemented in VASP). For a given migration mechanism, we then calculated activation barriers in different lithium-vacancy environments, and used these values to obtain kinetically resolved activation barriers ΔE_{KRA} given by Eq. (14). As described in Sec. II B, we then cluster expanded the ΔE_{KRA} with a local cluster expansion. This local cluster expansion together with the cluster expansion for the configurational energy of $O3$ constructed in Ref. 19, was then used to calculate the activation barrier ΔE_a in any local lithium-vacancy environment with Eq. (15). We then implement this procedure of calculating activation barriers in kinetic Monte Carlo simulations to calculate lithium diffusion coefficients using the equations of Secs. II A and II B. The following sections describe the results of these steps in detail.

A. First principles activation barriers

In this section, we investigate the dependence of activation barrier on the lithium-vacancy arrangement. We find that two qualitatively different hopping mechanisms exist depending on the immediate local environment around the hopping lithium ion. These are illustrated in Fig. 3. The first hopping mechanism occurs when the two lithium sites *a* and *b* [Fig. 3(a)] adjacent to the end points of the hop are occupied by lithium ions. The diffusing lithium ion then migrates along a path that closely follows the shortest path connecting the initial site of the hop and the vacancy. This shortest path, denoted by the arrow in Fig. 3(a), passes through a dumbbell of oxygen ions. We refer to this migration path as an oxygen dumbbell hop (ODH). This is the mechanism by which isolated vacancies exchange with lithium. When either one or both of the sites immediately adjacent to the end points of the hop are vacant, lithium migrates along a curved path which passes through a tetrahedral site as illustrated in Fig. 3(b). For this migration mechanism to occur, the destination of the hopping lithium ion must be part of a divacancy (it could also be part of a cluster of vacancies containing more than two vacancies). We refer to this migration mechanism as a tetrahedral site hop (TSH).

In Secs. III A 1–III A 3, we describe first principles calculations that form the basis of the above picture of lithium migration in Li_xCoO_2. Energies of activated states were calculated in supercells of Li_xCoO_2 containing 12 Li_xCoO_2 formula units. The number of ions in this supercell ranges between 47 to 37 depending on the lithium concentration (which was varied between $x=11/12$ to $x=1/12$). The $\vec{A}$ and $\vec{B}$ axes of the supercell form a $2\sqrt{3}\times 2\sqrt{3}$ two-dimensional superlattice in terms of the basal plane vectors $\vec{a}$ and $\vec{b}$ of the hexagonal unit cell of Li_xCoO_2. The $\vec{C}$ axis of the supercell

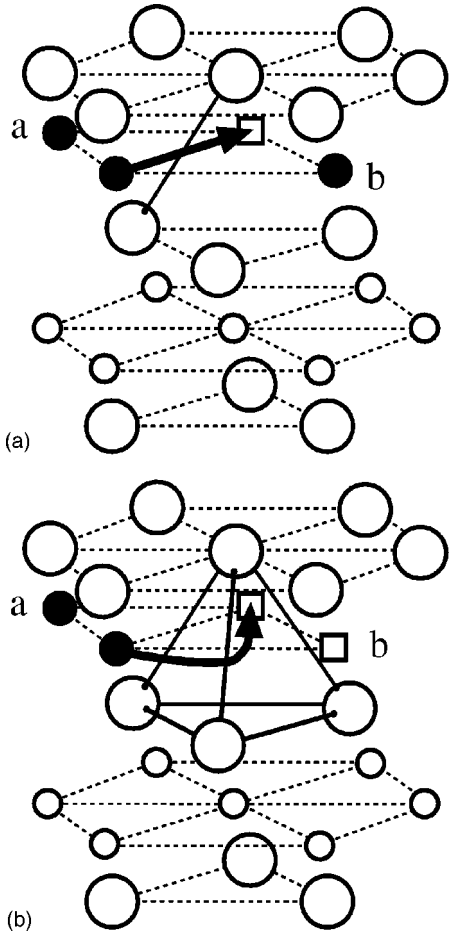

FIG. 3. Two different migration paths for lithium exist in Li_xCoO_2 depending on the local environment. (a) The oxygen dumbbell hop (ODH) occurs when sites *a* and *b* are occupied. (b) The tetrahedral site hop (TSH) occurs when at least one site adjacent to the end point of the hop is vacant. Large circles are oxygen, filled circles are lithium, squares are lithium vacancies and small empty circles are cobalt.

connects adjacent lithium planes and was chosen to be as shallow as possible to maximize the distance between the periodic images of the hopping lithium ions in adjacent lithium planes. The coordinates of the supercell vectors in terms of the hexagonal unit cell vectors of Li_xCoO_x are listed in Table I. Calculations of activation barriers were also performed in a 16 Li_xCoO_2 formula unit supercell. In all supercell calculations, we used a $2\times2\times2$ k-point mesh which is equivalent to eight irreducible *k* points.

TABLE I. The $\vec{A}$, $\vec{B}$, and $\vec{C}$ cell vectors of the supercell in which the activation barriers were calculated. The vectors are expressed in terms of the conventional hexagonal setting of the $O3$ layered crystal structure.

$\vec{A}$	4.0	2.0	0.0
$\vec{B}$	−2.0	2.0	0.0
$\vec{C}$	0.333	1.666	0.333

In all calculations of the activation barriers, the volume of the supercell was linearly interpolated between the equilibrium volumes of the end points of the hop. During relaxations of the atomic positions, the volume was held fixed. Defect calculations in relatively small supercells converge more rapidly when the volume is held fixed than when the volume is allowed to relax.[73] The volumes of the end-point configurations, however, were fully relaxed.

1. Migration of a vacancy in $LiCoO_2$

Insight about hopping mechanisms can be obtained by investigating lithium migration in the dilute extremes of lithium concentration. One dilute extreme is migration of a single vacancy in an otherwise fully lithiated Li_xCoO_2 host. Figure 4(a) illustrates a projection of a lithium plane and the two adjacent oxygen planes. With the pseudopotential method in combination with the elastic band method, we find that a lowest energy migration path between adjacent octahedral sites closely follows the arrow A-B of Fig. 4(a). Although in the figure, the arrow A-B forms a straight line connecting adjacent octahedral sites, the actual migration path is slightly curved, but passes very close to the center of the oxygen dumbbell formed by the oxygen ions O_1 and O_2. Because of this, we refer to this migration path as an oxygen dumbbell hop (ODH). The activation barrier for the movement of an isolated vacancy through the ODH mechanism in an otherwise fully lithiated host is predicted to be 830 meV and the energy along this path is illustrated in Fig. 5(a).

The energy of the migrating lithium ion placed exactly at the center of the oxygen dumbbell [between O_1 and O_2 of Fig. 4(a)] is only 10 meV higher than at the true activated state which is slightly shifted towards an adjacent tetrahedral site. This suggests that a reasonable approximation for the activation barrier for the ODH can be obtained by assuming the activated state to be exactly at the center of the oxygen dumbbell.

2. Migration of isolated lithium in dilute Li_xCoO_2

Another dilute extreme is the migration of an isolated lithium ion between two octahedral sites in the lithium planes of CoO_2. A calculation with the elastic band method shows that the lowest energy path between adjacent octahedral sites is along the arrow with end points A-B of Fig. 4(b). As is evident from Fig. 4(b), this migration path passes through an adjacent tetrahedral site making this a tetrahedral site hop (TSH). The energy along the TSH is illustrated in Fig. 5(a). The plot clearly shows that the activation barrier for migration of an isolated lithium ion is exactly at the tetrahedral site. The value of the activation barrier is close to 600 meV.

It is striking that the maximum along the TSH path occurs at the center of the tetrahedral site, a relatively open space, instead of at the centers of the oxygen triangles forming the faces of the tetrahedral site. The explanation is electrostatic in origin. The tetrahedral site shares a face with an oxygen octahedra surrounding a Co ion. The large electrostatic repulsion between lithium and the positively charged Co ion energetically penalizes the position at the center of the tetra-

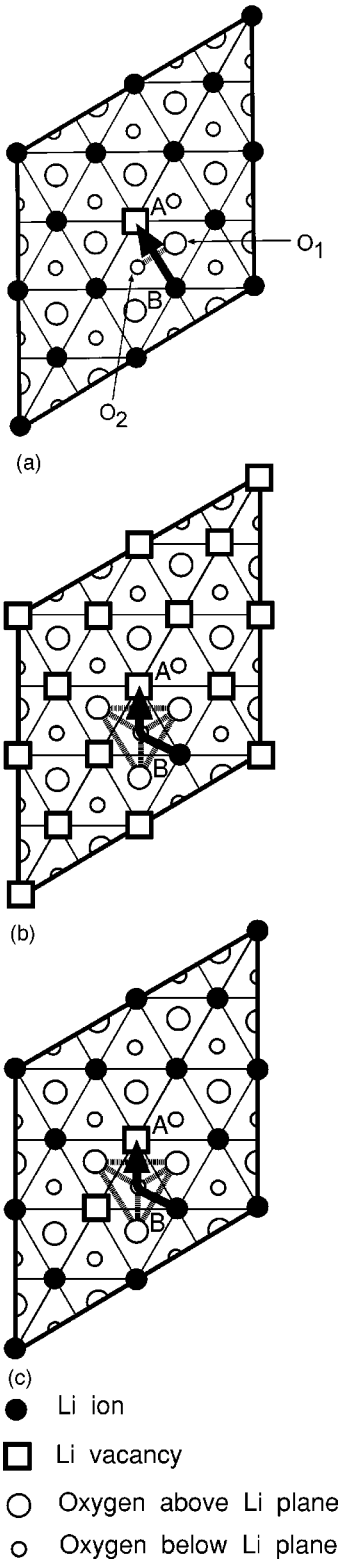

FIG. 4. Lithium migration paths in Li_xCoO_2 determined with the elastic band method. The triangular lattice corresponds to the lithium sites and the filled circles are lithium ions. The large empty circles are oxygen ions above the lithium plane and the small empty circles are oxygen ions below the lithium plane. See text for discussion.

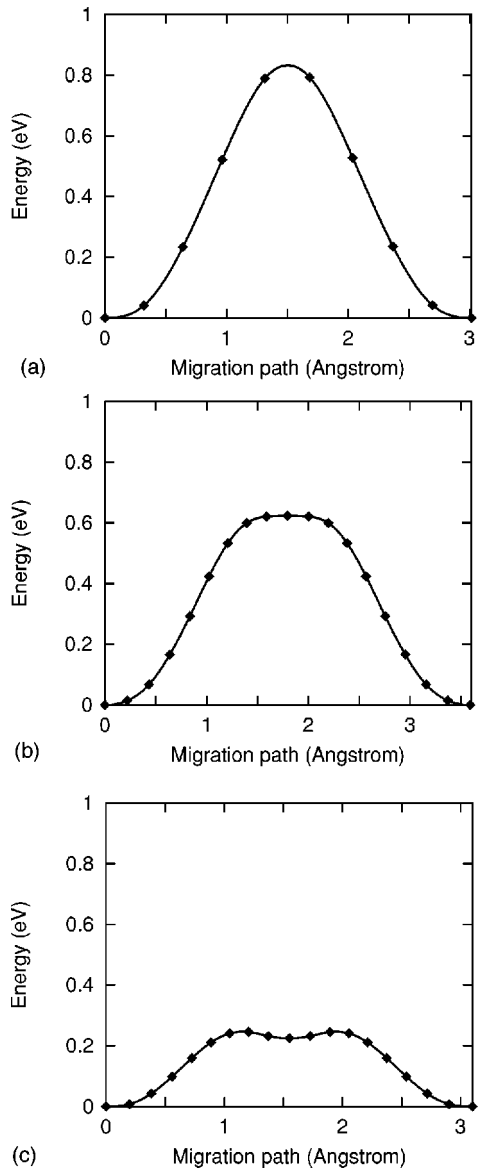

FIG. 5. Energy along the migration path in different lithium-vacancy environments determined with the elastic band method. Refer to Fig. 4 for the corresponding lithium-vacancy environments. (a) Migration of an isolated vacancy at $x=11/12$. (b) Migration of an isolated lithium according to a TSH at $x=1/12$ (c) Migration of a lithium ion into a divacancy according to a TSH at $x=10/12$.

hedron. This is manifested by the prediction that the saddle point at the tetrahedral site is displaced away from the ideal position of the tetrahedral site in a direction away from the cobalt ion and toward one of the oxygen ions forming the tetrahedron. As a result three lithium-oxygen bonds have a distance of 1.85 Å while the fourth lithium-oxygen bond has a distance of 1.53 Å.

The qualitative difference between the TSH and the ODH can be attributed to the absence or presence of lithium in the sites adjacent to the end points of the hop (sites *a* and *b* of Fig. 3). Once lithium ions occupy both sites *a* and *b* of Fig. 3 adjacent to the hop, the electrostatic repulsions due to these lithium ions displace the saddle point away from the sterically more attractive tetrahedral site towards a position almost at the center of the oxygen dumbbell.

3. Migration in an intermediate environment

At nondilute lithium concentrations, local arrangements will occur that are intermediate to those of the two dilute extremes. Figure 4(c) illustrates a particular arrangement around a hopping lithium ion that has features of the two dilute cases treated in Secs. III A and III B: one lithium site that simultaneously neighbors both end points of the hop is occupied, while the other lithium site is empty. Applying the elastic band method to this intermediate arrangement, we find that the migration path follows the arrow A-B of Fig. 4(c). This path passes through the tetrahedral site and can therefore be called a TSH.

Despite also passing through a tetrahedral site, the energetics of this migration path exhibits a subtle difference with the TSH for an isolated lithium ion in an empty CoO_2 host (Sec. III B). The energy along the path A-B of Fig. 4(c) is illustrated in Fig. 5(c). The tetrahedral site is no longer a maximum along the migration path, but a weak minimum. The activated state has shifted to a position closer to the center of the triangle of oxygen ions that form the face between the tetrahedral site and octahedral site. The barrier, however, is only about 25 meV higher than the energy of lithium at the tetrahedral site.

The difference between the energetics of the TSH of Figs. 4(b) and 4(c), is a result of a difference in the overall lithium concentration. The TSH of Fig. 4(c) occurs at high Li concentration (within the supercell, $x=0.8333$) while that of Fig. 4(b) occurs at very low lithium concentration. As was shown in previous first principles investigations of Li_xCoO_2, as more lithium is added to the CoO_2 host, the electron donated by lithium to the host is transferred to the oxygen ions.[74] The increased negative charge on the oxygen ions at high lithium concentration screens the electrostatic repulsion between the lithium at the tetrahedral site and the adjacent cobalt ion. This is qualitatively equivalent to saying that the effective charge on cobalt at high lithium concentration is $+3$ while at low x it is closer to $+4$. The electrostatic repulsion between cobalt and a lithium in a tetrahedral site therefore increases with decreasing lithium concentration.

4. General configuration dependence of activation barrier

The above results allow us to distinguish between two different migration mechanisms, the TSH and the ODH. Whether or not a TSH or ODH mechanism can occur depends on the lithium-vacancy arrangement in the immediate environment of the hopping lithium. If the two lithium sites that simultaneously neighbor the end points of the hop are occupied, lithium migration will occur along a path close to the ODH path. If both lithium sites adjacent to the hop are vacant, lithium will then migrate along one of the two TSH paths. And finally, if only one of the adjacent lithium sites are occupied, lithium migration will occur along the TSH passing by the empty lithium site.

Not only does the hopping mechanism depend on the local environment, but the value of the activation barrier for a

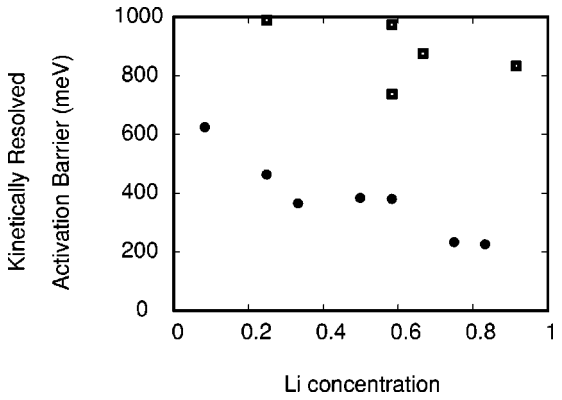

FIG. 6. Values for the kinetically resolved activation barriers, ΔE_{KRA}, at different lithium concentrations and arrangements in the $O3$ form of $\mathrm{Li}_x\mathrm{CoO}_2$. Filled circles correspond to TSH's and the squares correspond to ODH's.

given hopping mechanism will also depend on the surrounding lithium-vacancy arrangement. To determine this dependence, we have calculated the activation barriers at several lithium concentrations and in different local lithium-vacancy arrangements. Figure 6 illustrates the kinetically resolved activation barriers ΔE_{KRA} as defined by Eq. (14) at different lithium concentrations and local environments. The filled circles correspond to TSH activation barriers and the squares correspond to ODH activation barriers. Note that for the TSH, the number of end points n of the hop appearing in Eq. (14) is 3 and for the ODH n is equal to 2.

In the calculation of the kinetically resolved activation barriers ΔE_{KRA} for the TSH's, E_{AS} of Eq. (7) was set equal to the energy of lithium in the tetrahedral site along the TSH path. While for low lithium concentration, this approach yields the exact activation barrier (within the limit of the supercell method), for higher lithium concentrations, it leads to an approximation since the activated state is slightly shifted away from the tetrahedral site at high x (see Sec. III A 3). Nevertheless, as is clear in Fig. 5(b), the error is at most of the order of 25 meV or 10% for the TSH activation barrier at $x=0.8333$. For the ODH's, E_{AS} of Eq. (14) was set equal to the energy of the hopping lithium ion placed exactly at the center of the oxygen dumbbell. Although the actual saddle points for the ODH are slightly shifted away from the center of the oxygen dumbbell in a direction perpendicular to the hop direction, as noted in Sec. III A 1, we found that the error of this approximation is of the order of 10 meV.

The calculated activation barriers of Fig. 6 convey two major trends. First, the activation barriers for the ODH are almost twice as large as those of the TSH. This is not surprising, since the activated state of the ODH is sterically more constricted than that of the TSH. Furthermore, the ODH mechanism only occurs when the two lithium sites simultaneously neighboring the end points of the hop are occupied. The electrostatic repulsion between these adjacent lithium ions and the hopping lithium ion constitutes an additional energetic penalty to the activated state which is absent in the TSH mechanism.

The second trend in Fig. 6 is the increase in the activation barrier for the TSH as the lithium concentration is reduced. The activation barriers for the TSH vary relatively little at intermediate lithium concentration, however, at low lithium concentration, the TSH activation barrier increases by a significant amount. This increase is caused by the large contraction of the c-lattice parameter of the CoO_2 host frame work below $x=0.3$, a feature of $\mathrm{Li}_x\mathrm{CoO}_2$ that has both been measured experimentally[69,70] and has been predicted from first principles.[19] The contraction is accompanied by a reduction in the distance between the oxygen planes adjacent to the lithium planes which in turn causes a contraction of the tetrahedral site. To expose the role of the c-lattice parameter on the activation barrier, we artificially constrained the c-lattice parameter of the structure at $x=0.0833$ to have a value typical of that in the concentration range of $x=0.3$ and 0.6 and recalculated the activation barrier. The activation barrier decreases to 450 meV which is of the order of the activation barriers obtained at intermediate lithium concentration.

The general decrease in activation barrier above $x=0.5$ cannot be attributed to a c-lattice parameter variation since it is more or less constant in this concentration range. Instead it can be traced to the enhanced charge transfer to oxygen as x is increased. The higher electron density on oxygen screens the lithium in the tetrahedral site from the cobalt ion in an adjacent face-sharing octahedral site. This tends to make the tetrahedral site less unfavorable for lithium than at low lithium concentration.

To obtain an estimate of the supercell convergence error for the activation barriers, we calculated the activation barriers for the TSH at $x=1/2$ and the ODH at infinite vacancy dilution in a supercell containing 16 $\mathrm{Li}_x\mathrm{CoO}_2$ formula units. For the TSH at $x=1/2$, we found that the activation barrier changes by less than 30 meV. For the ODH with only one vacancy in the supercell, we found that the activation barrier changes by less than 70 meV. This suggests that the accuracy of the TSH activation barriers is better than that of the ODH.

B. Local cluster expansion of activation barriers

Many more possible local arrangements around a migrating lithium ion exist than were considered in the previous section. With the above kinetically resolved activation barriers, a local cluster expansion can be parametrized that will approximate the kinetically resolved activation barriers for other local environments.

The TSH and ODH mechanisms, which occur in different environments are characterized by distinct features; they have a different number of end points and the values of their respective activation barriers differ by a factor of 2. It is therefore natural that the activation barriers of both mechanisms should be parametrized with a separate cluster expansion.

In the present study, we only constructed a cluster expansion for the kinetically resolved activation barriers of the TSH. Since the activation barriers of the ODH are much larger than those of the TSH, the former mechanism will only be prevalent when the number of available TSH's are negligible. This, as will be borne out by the Monte Carlo results presented in the next section, only occurs at very dilute vacancy concentrations. In this regime, there is essen-

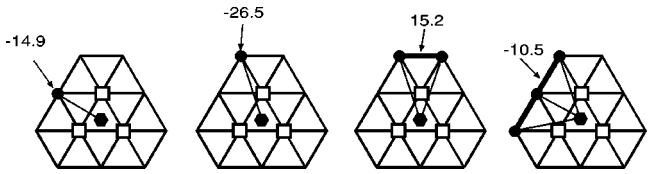

FIG. 7. Local cluster expansion of the kinetically resolved activation barrier ΔE_{KRA} for the TSH mechanism. The triangular lattice corresponds to lithium sites, and the squares correspond to the end points of the hop which are vacant when lithium is at the activated state. The filled hexagon corresponds to the tetrahedral site along the TSH migration path. The local cluster expansion includes two point clusters, a nearest neighbor cluster and a triplet cluster. The numerical values of the KECI are in units of meV. The KECI of the empty cluster V_0 is 411.3 meV.

tially one local configuration in the immediate vicinity of the the ion undergoing an ODH, namely, all lithium sites occupied. The activation barrier for the ODH can then be approximated by a single value, i.e., that calculated in the limit of dilute vacancy concentration.

A local cluster expansion containing five KECI was constructed for the kinetically resolved activation barriers of the TSH. The KECI were determined by performing a fit to the seven TSH activation barriers illustrated in Fig. 6. The root mean square error between the seven activation barriers calculated with the cluster expansion and the values obtained with the pseudopotential method is 40 meV. The clusters used in the expansion are illustrated in Fig. 7 and consist of the empty cluster V_0, the nearest and next nearest neighbor point clusters, a nearest neighbor pair cluster and a triplet cluster.

C. Calculated diffusion coefficients and related properties

Although knowledge of the different hopping mechanisms and their corresponding activation barriers is an essential ingredient in the calculation of the lithium diffusion coefficient, it is not sufficient. The diffusion coefficient also reflects the degree of correlation between the hopping lithium ions. This correlation is both thermodynamic, as manifested by the degree of short- or long-range order, as well as dynamic and can be captured simultaneously with kinetic Monte Carlo simulations.

In the kinetic Monte Carlo simulations, all energetics were calculated using cluster expansions. As was described in Sec. II A, the activation barrier ΔE_a appearing in the expression for the hop frequencies Γ_j [see Eq. (8)], can be decomposed into a sum of a kinetically resolved activation barrier ΔE_{KRA}, and configurational energies E_{e_j}, of the solid when the migrating ion resides at end point e_j of the hop [see Eq. (15)]. The cluster expansion for the $\mathrm{Li}_x\mathrm{CoO}_2$ in the $O3$ host, derived previously,[19] was used to calculate the E_{e_j}. For the TSH mechanism ΔE_{KRA} was calculated with the local cluster expansion discussed in Sec. III B. For the ODH, ΔE_{KRA} was set equal to 830 meV, the calculated activation barrier for the ODH in the dilute vacancy concentration limit.

The prefactor ν^* Eq. (11) in the expression for Γ [Eq. (8)] sets the time scale in the kinetic Monte Carlo simulations. Although the prefactor has a configurational dependence, we have neglected this dependence and have assumed a constant value for ν^* for all hops. Due to current computational limitations, no attempt was made to quantitatively determine prefactors for lithium diffusion in $\mathrm{Li}_x\mathrm{CoO}_2$ and we will plot $(10^{13}/\nu^*)D$. This quantity should correspond to the true values for D within one to two orders of magnitude.

The kinetic Monte Carlo simulations were performed with cells containing either 1944 or 7776 lithium sites (the actual number of lithium ions in the Monte Carlo cell can be determined by simply multiplying the concentration of lithium ions x with the number of lithium sites). At fixed temperature and lithium concentration, we performed the following sequence of steps. (i) First we performed 1000 canonical Monte Carlo steps to generate a representative equilibrium lithium-vacancy arrangement. The last lithium-vacancy arrangement of this canonical Monte Carlo simulation was used as the starting configuration for the kinetic Monte Carlo simulations. (ii) Next, in the kinetic Monte Carlo simulations, we performed between 500 to 1000 KMCS using the algorithm described in Sec. II D. The last 300 to 500 of these steps were used for time averaging as described in Ref. 64. At each temperature and concentration, this sequence of steps was repeated 50 times whereby the final configuration of the kinetic Monte Carlo simulation of step (ii) was used as the initial configuration of the canonical Monte Carlo simulation of step (i). This ensured that each of the 50 kinetic Monte Carlo simulations started with a different initial lithium-vacancy configuration representative of equilibrium conditions. The repetition of the above two steps by 50 was necessary to obtain sufficiently uncorrelated data for the averages of D_J and D^*. The thermodynamic factor Θ given by Eq. (4) was calculated with grand-canonical Monte Carlo simulations as described in Ref. 19.

1. Diffusion coefficients

Figures 8(a) and 8(b) show calculated values for the diffusion coefficients D_J and D^* at 300 and 400 K. It is clear that the diffusion coefficients vary within several orders of magnitude with lithium concentration. At high lithium concentration, the diffusion coefficients are very low, increasing by almost two orders of magnitude as the lithium concentration x is reduced to approximately 0.6. For small x, the diffusion coefficients are again very low. The significant dips in D_J and D^* around $x=1/3$ and $x=1/2$ at 300 K and around $x=1/2$ at 400 K are the result of lithium ordering. The cluster expansion for the configurational energy of the $O3$ form of $\mathrm{Li}_x\mathrm{CoO}_2$ predicts lithium ordering at $x=1/2$ and $x=1/3$ with approximate order-disorder transition temperatures of 430 and 380 K, respectively.[19] In the ordered phase at $x=1/2$, the lithium ions order in rows separated by rows of vacancies while at $x=1/3$ the lithium ions order according to a $\sqrt{3}\times\sqrt{3}$ superlattice. The occurrence of these ordering transformations can best be represented in a phase diagram which for the $O3$ form of $\mathrm{Li}_x\mathrm{CoO}_2$ was done in Ref. 19. In real systems ordering may be somewhat less perfect than in the simulations, making the dips in D_J and D^* less pronounced. Notice that D_J and D^* have the same order of magnitude yet they do not equal each other.

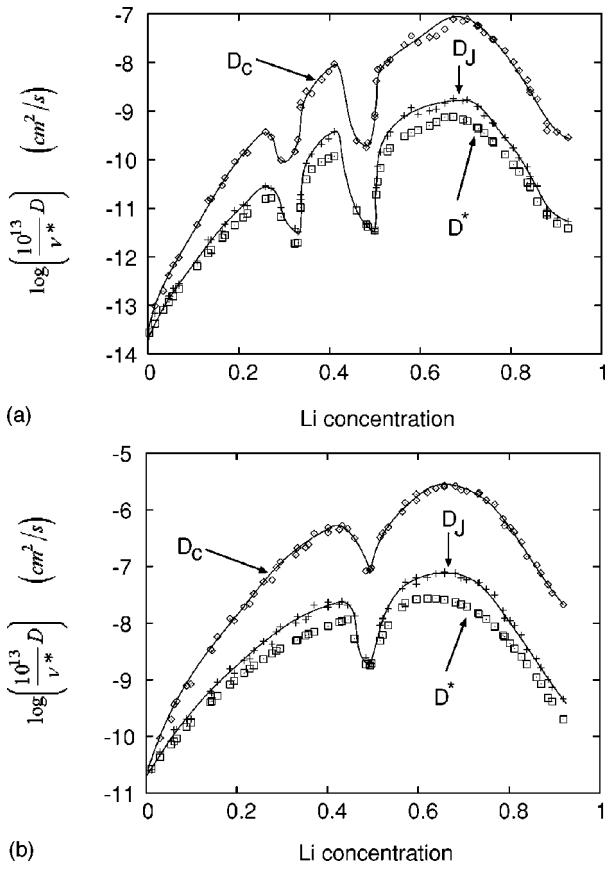

FIG. 8. Calculated lithium diffusion coefficients for Li_xCoO_2 at (a) 300 K and (b) 400 K. Because of the uncertainty in ν^* of Eq. (11) we plot $(10^{13}/\nu^*)D$ where D is either D_c, D_J, or D^* and is expressed in cm^2/s.

The chemical diffusion coefficient D_c which determines macroscopic diffusion as defined by Fick's law [Eq. (2)] is equal to the product of D_J with the thermodynamic factor [Eq. (4)]. Figure 9 illustrates the thermodynamic factor for the $O3$ form of Li_xCoO_2 at 300 K.

Note that D_J and Θ give opposite effects of ordering on D_c. Near the ordered stoichiometries, Θ is large, enhancing the chemical diffusion coefficient. D_J on the other hand

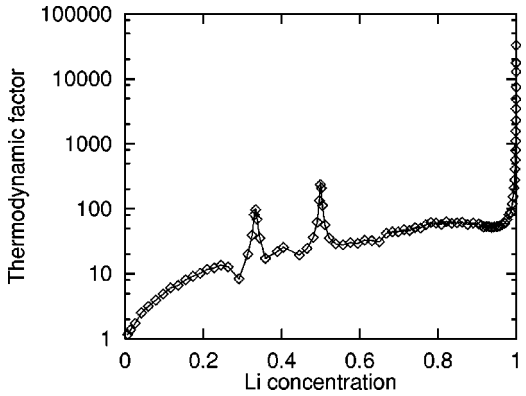

FIG. 9. The calculated thermodynamic factor Θ at 300 K. Θ measures the deviation from ideality of the system and is given by Eq. (4).

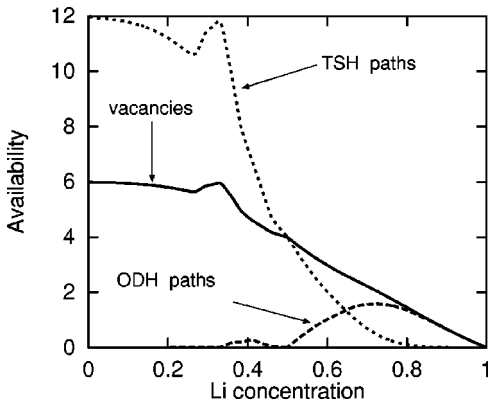

FIG. 10. The average availability of TSH pathways, ODH pathways and vacancies per lithium ion as a function of lithium concentration.

drops by several orders of magnitude at these stoichiometries, reflecting the fact that ordering ''locks up'' the vacancies needed for diffusion. In this system, D_J clearly dominates and the overall D_c also has a minimum. Due to a very asymmetric minimum in D_J (which occurs exactly at $x=1/2$ and $x=1/3$) and a symmetric thermodynamic factor around those same compositions, the exact minima in D_c arise at x slightly less than 1/2 or 1/3.

If the maximum in Θ were stronger or the minimum in D_J weaker, it is possible to obtain a maximum in D_c near the ordered stoichiometries. This may for example be the case when partial ordering occurs due to other defects in the material (impurities, oxygen or cobalt vacancies).

2. Microscopic hopping behavior

In the kinetic Monte Carlo simulations, both the TSH and ODH mechanims are considerd. The frequency with which either hop mechanism occurs is proportional to the *availability* of the particular mechanism multiplied by the exponent of the negative of the activation barrier divided by kT. Figure 10 illustrates the average availability of TSH and ODH mechanisms per lithium ion as a function of lithium concentration. Also illustrated is the average number of vacancies adjacent to a lithium ion normalized per lithium ion. At low x, the availability of TSH's is high while that of ODH's is very low. Above about $x=0.65$, however, the number of candidate ODH paths accessible to each lithium increases and exceeds the availability of TSH paths. The TSH mechanism requires at least a divacancy adjacent to the hopping lithium ion and at high lithium concentration, the concentration of divacancies is less than the concentration of single vacancies. In fact, if the lithium ions and vacancies are randomly distributed, the concentration of divacancies scales as $(1-x)^2$ while that of single vacancies as $(1-x)$. Since vacancies repel each other as x approaches 1, the concentration of divacancies is even lower than $(1-x)^2$ in Li_xCoO_2. The crossover in the availability of TSH paths versus ODH paths suggests that at low lithium concentration, the TSH mechanism will dominate and at high lithium concentration the ODH

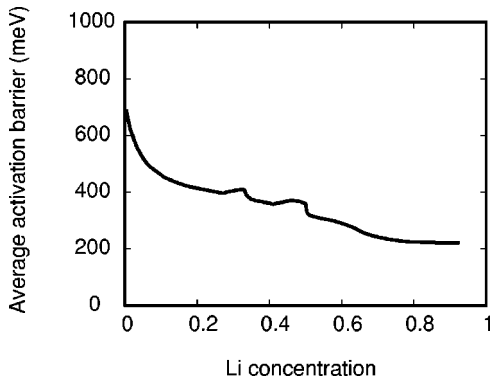

FIG. 11. Variation with x of the average activation barrier overcome by hopping lithium ions in the kinetic Monte Carlo simulations.

mechanism should dominate. The transition between the TSH and ODH mechanism can be estimated by the value of x for which

$$a_{\mathrm{TSH}}\nu^* \exp\left(\frac{-\Delta E_a^{\mathrm{TSH}}}{kT}\right) = a_{\mathrm{ODH}}\nu^* \exp\left(\frac{-\Delta E_a^{\mathrm{ODH}}}{kT}\right), \tag{19}$$

where a_{TSH} and a_{ODH} are the average availabilities of the TSH and ODH mechanisms and where $\Delta E_a^{\mathrm{TSH}}$ and $\Delta E_a^{\mathrm{ODH}}$ are representative activation barriers for the respective mechanisms. At this concentration x, the TSH and ODH mechanisms occur with equal frequency. Using values for a_{TSH} and a_{ODH} from grand canonical Monte Carlo simulations and typical activation barriers for the two mechanisms, we find that the transition from the TSH to the ODH mechanism occurs at infinite vacancy dilution, implying that the TSH mechanism always dominates. This was also predicted by the kinetic Monte Carlo simulations.

The average activation barrier $\langle \Delta E_a \rangle$ as experienced by hopping lithium ions is illustrated in Fig. 11. Since lithium ions hop according to the TSH mechanism between $x=0$ and 1, $\langle \Delta E_a \rangle$ naturally follows the same trend of the first principles values of ΔE_{KRA} of Fig. 6, i.e., increasing $\langle \Delta E_a \rangle$ with decreasing x.

The large variations in D_c with x are closely linked to the variation in activation barrier and availability of the TSH mechanism with x. At dilute x, the activation barrier is high resulting in a small diffusion coefficient. As x increases, the activation barrier progressively decreases producing an increase in the diffusion coefficient. The dips in diffusivity around $x=1/3$ and $x=1/2$ are a result of lithium ordering which from an energetic point of view tends to lock the lithium ions in their sublattice sites. Further increase of x above 1/2 results in a decrease in the diffusion coefficient, even though the average activation barrier levels off. This reduction of D_c is a result of a decline in the number of available vacancies to hop to in combination with an even more rapid decline in the average number of available TSH paths to enable lithium hops to neighboring vacancies.

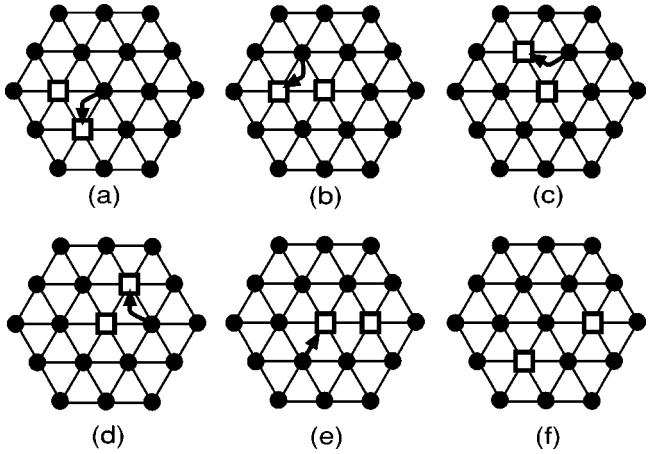

FIG. 12. At high lithium concentration, lithium migration according to the TSH mechanism occurs through the cartwheel motion of a divacancy.

3. Correlation factor

The prevalence of the TSH mechanism for most values of x has interesting implications about the correlated motion of the lithium ions. The above results indicate that lithium migration in layered Li_xCoO_2 is mediated through clusters of divacancies since they enable lithium ions to hop according to the TSH mechanism. While at low lithium concentrations, divacancies are sufficiently abundent, at high x clusters of vacancies are energetically and entropically less favored than a uniform distribution of single vacancies. Nevertheless, even for high x a preponderance of lithium hops occur through divacancies.

To better understand the implications of divacancy diffusion, it is useful to consider the motion of an isolated divacancy. Figure 12(a) illustrates a cluster of two vacancies surrounded by lithium ions in the immediate environment. Figures 12(a)–12(e) shows that the effect of lithium diffusion according to the TSH mechanism (as illustrated by the curved arrows), is to rotate the divacancy similar to the movement of a cartwheel. Only on rare occasions after the occurrence of an ODH do the vacancies of the divacancy cluster separate. The latter case is illustrated in Figs. 12(e) and 12(f) and has a very low probability of occurrence due to the high activation barrier associated with the ODH mechanism.

A measure of correlated motion is the correlation factor which is defined as

$$f = \frac{\langle \vec{r}(t)^2 \rangle}{na^2}, \tag{20}$$

where $\langle \vec{r}(t)^2 \rangle$ is the average distance squared that a lithium ion has travelled after time t, n is the average number of hops that a lithium ion has performed, and a is the distance associated with a hop. The correlation factor f measures the deviation of the lithium intrinsic diffusion coefficient D^* from that of an equal number of random walkers on a triangular lattice. When lithium migration is uncorrelated, the correlation factor equals one. This occurs as x approaches

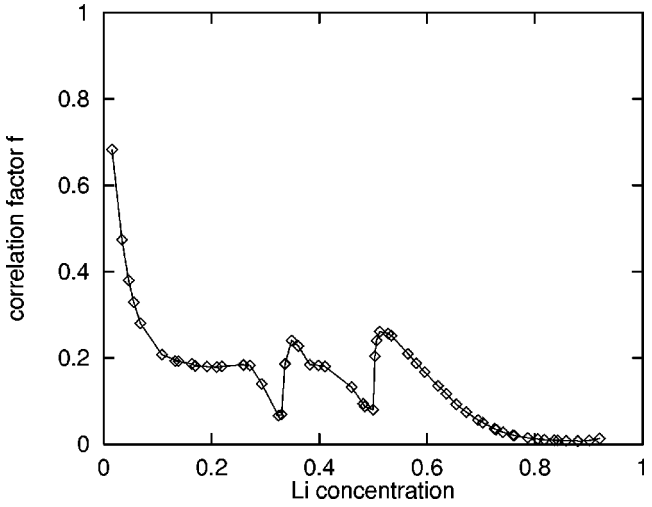

FIG. 13. Calculated correlation factor as a function of lithium concentration at 300 K.

zero since the interactions among different lithium ions disappear and migration of isolated lithium ions becomes that of a random walk. As x approaches one, the motion of the isolated vacancies becomes that of a random walk, however, migration of the lithium ions does not. The theoretical value of f as x approaches 1.0 on a triangular lattice is to first approximation 2/3.[76]

Figure 13 illustrates the correlation factor for lithium diffusion in Li_xCoO_2 as a function of x at 300 K. Although f approaches the theoretical value in the dilute limit of $x=0$, at intermediate x, it deviates strongly from a linear interpolation between $f=1$ at $x=0$ and $f=2/3$ at $x=1$. In fact, as x approaches 1, f remains very low. Only once the ODH mechanism dominates at infinite vacancy dilution whereby lithium exchanges with isolated vacancies will f approach the value of 2/3. Figure 13 clearly illustrates that the TSH hop mechanism results in significant correlated motion of the lithium ions, and thereby reduces the diffusivity from what it would be for a random walk.

D. Discussion

In this paper, we have presented a formalism for the first-principles study of diffusion in systems with configurational disorder. The procedure entails three steps: (i) a systematic first-principles investigation of migration mechanisms and their activation barriers in the presence of different configurations, (ii) the construction of cluster expansions to parametrize the configuration dependent activation barriers, and (iii) implementation of the cluster expansions in kinetic Monte Carlo simulations to obtain kinetic properties such as diffusion coefficients. A key feature of this formalism is the local parametrization of a kinetically resolved activation barrier. When implemented in a kinetic Monte Carlo simulation together with the standard configurational cluster expansion, an accurate model for the kinetic behavior of materials can be obtained. By construction this model has the correct ensemble averages and thermodynamic properties.

As an example, we have applied this approach for the study of lithium diffusion in Li_xCoO_2. First principles pseudopotential calculations within LDA have shown that two hopping mechanisms exist in Li_xCoO_2 depending on the local environment: the tetrahedral site hop (TSH) and the oxygen dumbbell hop (ODH) (Sec. III A). Furthermore, calculations of activation barriers for lithium migration in different lithium-vacancy environments have shown that the activation barrier can vary significantly with concentration and local configuration. These simulations have shown that of the two possible hopping mechanisms, the TSH mechanism dominates at all lithium concentrations, meaning that lithium diffusion is mediated by the motion of divacancies. Furthermore, the simulations predict that the diffusion coefficient has a strong concentration dependence.

A hopping mechanism involving an adjacent tetrahedral site has previously been conjectured from molecular dynamics simulations using empirical potentials.[75] The present systematic study of the environment dependence of the activation barriers using more realistic first-principles calculations has shown that in fact two migration paths exist depending on the immediate environment. More importantly, the present study has shown that the migration path through the tetrahedral site occurs only if the end point of the hop belongs to a divacancy. This is a significant constraint on the TSH mechanism, especially at high lithium concentration where the number of divacancies is severely limited. Moreover, as is evident from the calculated correlation factor, diffusion mediated by divacancies in Li_xCoO_2 is very inefficient. One of the advantages of a kinetic Monte Carlo simulation for the study of diffusion in configurationally disordered systems is that the system can be thermodynamically equilibrated and diffusion can be sampled over long times. These long-time regimes are currently inaccessible with molecular dynamics simulations. The subtle influences of lattice parameter variations and charge transfer from lithium to the Co-O complex on the activation barrier, also illustrate the importance of a quantum mechanical description of the energetics. It is unlikely that empirical potential methods as are often used in oxides would be able to capture this environment dependence of the activation barrier.

Several sources of inaccuracies in the calculated activation barriers can be identified that originate either from numerical errors or from approximations. Potential numerical inaccuracies arise from an inadequate k-point convergence and the use of a supercell. We estimate these errors to be of the order of 50–100 meV on the activation barriers. Nevertheless, since the same supercell and k-point mesh was used in the calculation of all activation barriers we expect this to be a systematic error. Another inaccuracy occurs at high lithium concentration. At large x, the activation barrier for the TSH is not at the tetrahedral site as was assumed in our calculations, but is slightly shifted away from the tetrahedral site as illustrated in Sec. III A 3. The error of this approximation is at most 25 meV and diminishes as x is reduced. Then there is the error resulting from the truncation of the local cluster expansion. While the least squares error between the first principles values for ΔE_{KRA} and those reproduced by the local cluster expansion of 40 meV is of the same order as those due to k-point and supercell convergence, the expansion has only a limited number of terms and

may therefore lack sufficient predictive power. Nevertheless, the average activation barrier calculated in the Monte Carlo simulation (Fig. 11) traces the same trend as the first principles values for ΔE_{KRA} of Fig. 13. This indicates that the local cluster expansion captures the essential physics of the concentration dependence of the activation barrier. Finally, an error that is more difficult to quantify, arises from the use of the local density approximation of density functional theory. Since hopping rates depend exponentially on the activation barrier, calculated diffusion coefficients are very sensitive to relatively small errors in activation barriers. A systematic error in the calculated activation barrier of 100 meV, a value that is not uncommon for first principles calculations, produces an error of two orders of magnitude in the diffusion coefficient at 300 K.

Due to computational limitations, we have not attempted to calculate a value for the prefactor ν^* given by Eq. (11) which appears in the hop frequency Γ of Eq. (8). Instead we have assumed a constant value for ν^* and have plotted calculated diffusion coefficients as $(10^{13}/\nu^*)\mathrm{D}$, where 10^{13} sec^{-1} is a reasonable estimate for ν^*. Although in general, the configuration dependence of ν^* is likely to be negligible, for $\mathrm{Li}_x\mathrm{CoO}_2$, this may not be the case. The prefactor depends on the local entropy of a lithium ion in an octahedral site and a lithium ion in the activated state. In the $\mathrm{Li}_x\mathrm{CoO}_2$, the latter value will be sensitive to concentration since the shape of the energy surface around the tetrahedral site varies qualitatively with lithium concentration [compare Figs. 5(b) and 5(c)]. Future studies should address the accurate calculation of the prefactor for diffusion in $\mathrm{Li}_x\mathrm{CoO}_2$ to clarify its importance in affecting the diffusion coefficient. In addition to assuming an environment independent ν^* we have also assumed a recrossing coefficient κ equal to unity. The recrossing coefficient is sensitive to the shape of the potential surface around the dividing surface[33,34] and we can expect it to differ from 1 especially at high lithium concentration where the energy along the migration path exhibits a slight local minimum.

Several experimental studies of the lithium diffusion coefficient in $\mathrm{Li}_x\mathrm{CoO}_2$ have been performed in recent years. The different measurements of D_c qualitatively exhibit a similar concentration dependence. Although, in Refs. 77,78, D_c is expressed as a function of voltage, the concentration dependence can be inferred by comparison with accurately calibrated voltage versus concentration curves. In Ref. 79, D_c is expressed as a function of concentration, however, comparison of their voltage versus concentration curves with those typically shown in the literature[68,69] suggest that the concentration scale in Ref. 79 is slightly expanded. Typically the lithium concentration attributed to 4.15 V is measured to be 0.5, while that reported in Ref. 79 is 0.3, suggesting that the amount of lithium assumed to have been removed from the $\mathrm{Li}_x\mathrm{CoO}_2$ during charging is overestimated in Ref. 79. After either making the conversions from voltage to concentration for the data of Refs. 77,78, or the necessary adjustments in concentration in Ref. 79, the basic trend in D_c can be summarized as follows. D_c drops by almost two orders of magnitude as x is increased between $x=0.5$ and 0.75. Between $x=0.75$ and 0.95, a two phase region exists and a value for D_c cannot be defined.

A recent experimental study by Jang *et al.*[80] showed that D_J exhibits a minimum as a result of lithium ordering at $x=1/2$, in qualitative agreement with the calculations in this work. The experimentally measured dip in D_J at $x=1/2$, however, is not as large as predicted in this work and the measured chemical diffusion coefficient D_c actually peaks due to the spike in Θ at $x=1/2$. The extent of the dip in D_J due to ordering is expected to increase with the stability of the ordered phase. The stability of the ordered phase at $x=1/2$ in $\mathrm{Li}_x\mathrm{CoO}_2$ at room temperature is predicted by the cluster expansion to be much stronger than observed experimentally.[19] In fact, the order-disorder transition temperature of this phase is overpredicted by 100 °C.[19] Furthermore, the stability of the ordered phase at $x=1/2$, measured experimentally, is significantly weakened by the presence of impurities,[81] suggesting that the degree of ordering in $\mathrm{Li}_x\mathrm{CoO}_2$ can vary from sample to sample. This complicates a comparison between the experimental and calculated values of D_c around $x=1/2$.

IV. CONCLUSION

In this paper, we have described a formalism to calculate diffusion coefficients from first principles in systems with significant configurational disorder. The link between first-principles total energy methods (such as density functional theory) and statistical mechanics methods such as kinetic Monte Carlo simulations lies in the cluster expansion formalism. We have extended this formalism to describe the configuration dependence of the activation barriers.

As an illustration, we have investigated lithium diffusion in layered $\mathrm{Li}_x\mathrm{CoO}_2$. Our calculations have shown that lithium ions can hop according to two migration paths depending on the local environment around the hopping ion. Furthermore, we have found that the activation barrier for a particular hopping mechanism can depend strongly on the local lithium-vacancy configuration. Kinetic Monte Carlo simulations predict that lithium diffusion in $\mathrm{Li}_x\mathrm{CoO}_2$ is mediated by divacancies even at high lithium concentrations where the concentration of divacancies is low. The simulations have also shown that the strong concentration dependence of the activation barrier results in a diffusion coefficient that spans several orders of magnitude with lithium concentration.

ACKNOWLEDGMENTS

The authors would like to thank Dr. Dane Morgan and Dr. Stephen Foiles for helpful discussions. This work was supported by the Department of Energy, Office of Basic Energy Sciences under Contract No. DE-FG02-96ER45571. This research was supported in part by NSF cooperative agreement ACI-9619020 through computing resources provided by the National Partnership for Advanced Computational Infrastructure at the San Diego Supercomputer Center. One of the authors (A.V.D.V.) gratefully acknowledges support from the U.S. DOE Computational Science Graduate Fellowship Program.

[1] S. C. Singhal, MRS Bull. **253**, 16 (2000).
[2] A. R. West, in *Solid State Electrochemistry*, edited by P. Bruce (Cambridge University Press, Cambridge, 1995), p. 7.
[3] J. B. Goodenough, in *Solid State Electrochemistry* (Ref. 2), p. 43.
[4] W. R. McKinnon, in *Solid State Electrochemistry* (Ref. 2), p. 163.
[5] W. Weppner, in *Solid State Electrochemistry* (Ref. 2), p. 163.
[6] M. M. Thackeray, J. O. Thomas, and M. S. Whittingham, MRS Bull. **253**, 39 (2000).
[7] J. M. Sanchez, F. Ducastelle, and D. Gratias, Physica A **128**, 334 (1984).
[8] D. de Fontaine, in *Solid State Physics*, edited by H. Ehrenreich and D. Turnbull (Academic Press, New York, 1994), p. 33.
[9] M. Sluiter, D. De Fontaine, X. Q. Guo, R. Podloucky, and A. J. Freeman, Phys. Rev. B **42**, 10 460 (1990).
[10] G. Ceder, M. Asta, W. C. Carter, M. Kraitchman, D. De Fontaine, M. E. Mann, and M. Sluiter, Phys. Rev. B **41**, 8698 (1990).
[11] J. M. Sanchez, J. P. Stark, and V. L. Moruzzi, Phys. Rev. B **44**, 5411 (1991).
[12] M. Asta, D. De Fontaine, M. Vanschilfgaarde, M. Sluiter, and M. Methfessel, Phys. Rev. B **46**, 5055 (1992).
[13] M. Asta, R. McCormack, and D. De Fontaine, Phys. Rev. B **48**, 748 (1993).
[14] Z. W. Lu, S.-H. Wei, A. Zunger, S. Forta-Pessoa, and L. G. Ferreira, Phys. Rev. B **44**, 512 (1991).
[15] R. Osorio, Z. W. Lu, S.-H. Wei, and A. Zunger, Phys. Rev. B **47**, 9985 (1993).
[16] A. Zunger, in *Statics & Dynamics of Alloy Phase Transformations*, edited by P. E. A. Turchi and A. Gonis (Plenum, New York, 1994), p. 361.
[17] P. D. Tepesch, A. F. Kohan, G. D. Garbulsky, G. Ceder, C. Coley, H. T. Stokes, L. L. Boyer, M. J. Mehl, B. P. Burton, K. J. Cho, and J. Joannopoulos, J. Am. Ceram. Soc. **79**, 2033 (1996).
[18] V. Ozolins, C. Wolverton, and A. Zunger, Phys. Rev. B **57**, 6427 (1998).
[19] A. Van der Ven, M. K. Aydinol, G. Ceder, G. Kresse, and J. Hafner, Phys. Rev. B **58**, 2975 (1998).
[20] G. Ceder and A. Van der Ven, Electrochim. Acta **45**, 131 (1999).
[21] A. Van der Ven and G. Ceder, Electrochem. Solid State Lett. **3**, 301 (2000).
[22] R. Gomer, Rep. Prog. Phys. **53**, 917 (1990).
[23] G. F. Mazenko, in *Surface Mobilities on Solid Materials*, edited by Vu Thien Binh (Plenum, New York, 1983), Vol. 86, p. 27.
[24] Y. Zhou and G. H. Miller, J. Chem. Phys. **100**, 5516 (1996).
[25] S. R. de Groot and P. Mazur, *Non-equilibrium Thermodynamics* (North-Holland, Amsterdam, 1962).
[26] C. Uebing and R. Gomer, J. Chem. Phys. **100**, 7759 (1994).
[27] G. DeLorenzi, C. P. Flynn, and G. Jacucci, Phys. Rev. B **30**, 5430 (1984).
[28] G. H. Vineyard, J. Phys. Chem. Solids **3**, 121 (1957).
[29] K. C. Pandey and E. Kaxiras, Phys. Rev. Lett. **66**, 915 (1991).
[30] E. Kaziras and K. C. Pandey, Phys. Rev. B **47**, 1659 (1993).
[31] E. Kaxiras and J. Erlebacher, Phys. Rev. Lett. **72**, 1714 (1994).
[32] C. H. Bennet, in *Diffusion in Solids: Recent Developments*, edited by A. S. Nowick and J. J. Burton (Academic, New York, 1975), p. 73.
[33] M. Toller, G. Jacucci, G. DeLorenzi, and C. P. Flynn, Phys. Rev. B **32**, 2082 (1985).
[34] M. Marchese, G. Jacucci, and C. P. Flynn, Phys. Rev. B **36**, 9469 (1987).
[35] A. F. Voter and J. D. Doll, J. Chem. Phys. **82**, 80 (1985).
[36] A. F. Voter, J. D. Doll, and J. M. Cohen, J. Chem. Phys. **90**, 2045 (1989).
[37] G. Ceder, Comput. Mater. Sci. **1**, 114 (1993).
[38] W. R. McKinnon and R. R. Haering, in *Modern Aspects of Electrochemistry*, edited by R. E. White, J. O. M. Backris, and B. E. Conway (Plenum, New York, 1983), Vol. 15, p. 237.
[39] J. W. D. Connolly and A. R. Williams, Phys. Rev. B **27**, 5169 (1983).
[40] G. D. Garbulsky and G. Ceder, Phys. Rev. B **51**, 67 (1995).
[41] D. B. Laks, L. G. Ferreira, S. Froyen, and A. Zunger, Phys. Rev. B **46**, 12 587 (1992).
[42] V. Ozolins, Ph.D. thesis, Royal Institute of Technology, Stockholm, Sweden, 1996.
[43] D. Morgan, J. D. Althoff, and D. de Fontaine, J. Phase Equilib. **19**, 559 (1998).
[44] A. Van der Ven, Ph.D. thesis, MIT, 2000.
[45] G. D. Garbulsky and G. Ceder, Phys. Rev. B **49**, 6327 (1994).
[46] V. Ozolins, C. Wolverton, and A. Zunger, Phys. Rev. B **58**, 5897 (1998).
[47] P. Hohenberg and W. Kohn, Phys. Rev. **136**, 864 (1964).
[48] W. Kohn and L. J. Sham, Phys. Rev. **140**, A1133 (1965).
[49] G. Kresse and J. Furthmüller, Phys. Rev. B **54**, 11 169 (1996).
[50] G. Kresse and J. Furthmüller, Comput. Mater. Sci. **6**, 15 (1996).
[51] M. C. Payne *et al.*, Rev. Mod. Phys. **64**, 1045 (1992).
[52] D. Vanderbilt, Phys. Rev. B **41**, 7892 (1990).
[53] G. Mills, H. Jonsson, and G. K. Schenter, Surf. Sci. **324**, 305 (1995).
[54] W. M. Young and E. W. Elcock, Proc. Phys. Soc. London **89**, 735 (1966).
[55] G. E. Murch and R. J. Thorn, J. Phys. Chem. Solids **38**, 789 (1977).
[56] G. E. Murch, Philos. Mag. A **43**, 871 (1981).
[57] M. Tringides and R. Gomer, Surf. Sci. **145**, 121 (1984).
[58] B. Fultz, J. Chem. Phys. **87**, 1604 (1987).
[59] H. C. Kang and W. H. Weinberg, J. Chem. Phys. **90**, 2824 (1989).
[60] C. Uebing and R. Gomer, J. Chem. Phys. **95**, 7626 (1991).
[61] L. Zhao, R. Najafabadi, and D. J. Srolovitz, Acta Mater. **44**, 2737 (1996).
[62] F. M. Bulnes, V. D. Pereyra, and J. L. Riccardo, Phys. Rev. E **58**, 86 (1998).
[63] A. B. Bortz, M. H. Kalos, and J. L. Lebowitz, J. Comput. Phys. **17**, 10 (1975).
[64] K. W. Kehr and K. Binder, in *Applications of the Monte Carlo Method in Statistical Physics*, edited by K. Binder (Springer-Verlag, Berlin, 1984), p. 181.
[65] K. Binder and D. W. Heermann, *Monte Carlo Simulations in Statistical Physics* (Springer-Verlag, New York, 1988).
[66] K. Mizushima, P. C. Jones, P. J. Wiseman, and J. B. Goodenough, Mater. Res. Bull. **15**, 783 (1980).
[67] H. J. Orman and P. J. Wiseman, Acta Crystallogr. **40**, 12 (1984).
[68] J. N. Reimers and J. R. Dahn, J. Electrochem. Soc. **139**, 2091 (1992).
[69] T. Ohzuku and A. Ueda, J. Electrochem. Soc. **141**, 2972 (1994).
[70] G. G. Amatucci, J. M. Tarascon, and L. C. Klein, J. Electrochem. Soc. **143**, 1114 (1996).
[71] M. Menetrier, I. Saadoune, S. Levasseur, and C. Delmas, J. Mater. Chem. **9**, 1135 (1999).

[72] A. Van der Ven, M. K. Aydinol, and G. Ceder, J. Electrochem. Soc. **145**, 2149 (1998).
[73] A. F. Kohan, G. Ceder, D. Morgan, and C. G. van de Walle, Phys. Rev. B **61**, 15 019 (2000).
[74] M. K. Aydinol, A. F. Kohan, G. Ceder, K. Cho, and J. Joannopoulos, Phys. Rev. B **56**, 1354 (1997).
[75] G. Nuspl, M. Nagaoka, K. Yoshizawa, F. Mohri, and T. Yamabe, Bull. Chem. Soc. Jpn. **71**, 2259 (1998).
[76] P. G. Shewmon, *Diffusion in Solids* (McGraw-Hill, New York, 1963).
[77] M. D. Levi, G. Salitra, B. Markovsky, H. Teller, D. Aurbach, Udo Heider, and Lilia Heider, J. Electrochem. Soc. **146**, 1279 (1999).
[78] J. M. McGraw, C. S. Bahn, P. A. Parilla, J. D. Perkins, D. W. Readey, and D. S. Ginely, Electrochim. Acta **45**, 187 (1999).
[79] J. Barker, R. Pynenburg, R. Koksbang, and M. Y. Saidi, Electrochim. Acta **41**, 2481 (1996).
[80] Y. I. Jang, B. J. Neudecker, and N. J. Dudney, Electrochem. Solid-State Lett. **4**, A74 (2001).
[81] J. N. Reimers, J. R. Dahn, and U. von Sacken, J. Electrochem. Soc. **140**, 2752 (1993).